Monthly Notices
of the
ROYAL ASTRONOMICAL SOCIETY

MNRAS **480,** 3812–3825 (2018)
Advance Access publication 2018 August 06

doi:10.1093/mnras/sty2131

On the influence of environment on star-forming galaxies

Lizhi Xie,[1]★ Gabriella De Lucia,[1] David J. Wilman,[2,3] Matteo Fossati,[2,3] Peter Erwin,[3] Leonel Gutiérrez[4] and Sandesh K. Kulkarni[3]

[1]*INAF - Astronomical Observatory of Trieste, via G.B. Tiepolo 11, I-34143 Trieste, Italy*
[2]*Universitäts-Sternwarte München, Scheinerstrasse 1, D-81679 München, Germany*
[3]*Max-Planck-Institut für Extraterrestriche Physik, Giessenbachstrasse, D-85748 Garching, Germany*
[4]*Instituto de Astronomía, Universidad Nacional Autónoma de México, Apdo. Postal 877, Ensenada, 22800 Baja California, Mexico*

Accepted 2018 July 28. Received 2018 July 28; in original form 2018 January 25

ABSTRACT

We use our state-of-the-art semi-analytic model for GAlaxy Evolution and Assembly (GAEA), and observational measurements of nearby galaxies to study the influence of the environment on the gas content and gaseous/stellar disc sizes of star-forming galaxies. We analyse the origin of differences between physical properties of satellites and those of their central counterparts, identified by matching the $V_{\rm max}$ of their host haloes at the accretion time of the satellites. Our model nicely reproduces the differences between centrals and satellites measured for the HI mass, size of the star-forming region, and stellar radii. In contrast, our model predicts larger differences with respect to data for the molecular gas mass and star formation rate. By analysing the progenitors of central and satellite model galaxies, we find that differences in the gas content arise after accretion, and can be entirely ascribed to the instantaneous stripping of the hot gas reservoir. The suppression of cold gas replenishment via cooling and star formation leads to a reduction of the cold gas and of its density. Therefore, more molecular gas is lost than lower density HI gas, and model satellites have less molecular gas and lower star formation rates than observed satellites. We argue that these disagreements could be largely resolved with the inclusion of a proper treatment for ram-pressure stripping of cold gas and a more gradual stripping of the hot gas reservoir. A more sophisticated treatment of angular momentum exchanges, accounting for the multi-phase nature of the gaseous disc, is also required.

Key words: galaxies: evolution – galaxies: ISM – galaxies: structure.

1 INTRODUCTION

It has long been known that galaxy properties correlate with their environment: galaxies in dense regions of the Universe are redder, more passive and more concentrated than those in regions with 'average' density (e.g. Dressler 1980; Balogh et al. 1999; Poggianti et al. 1999; Lewis et al. 2002; Gómez et al. 2003; Kauffmann et al. 2004; Bamford et al. 2009; Peng et al. 2012). Complementary trends are found if one focuses on the abundance of gas in galaxies (Bothun & Sullivan 1980; Chamaraux, Balkowski & Gerard 1980; Giovanelli & Haynes 1985; Solanes et al. 2001; Boselli, Lequeux & Gavazzi 2002; Boselli & Gavazzi 2006; Koopmann & Kenney 2004; Kenney, van Gorkom & Vollmer 2004; Chung et al. 2009; Jaffé et al. 2016; Odekon et al. 2016). H I deficiencies (i.e. the lack of H I with respect to isolated galaxies of similar morphological size and optical size) are typically ascribed to environmental effects. This hypothesis, however, is difficult to test as it would require, in principle, the identification of the progenitors of galaxies observed today, at a time when they were residing in similar environments.

Theoretically, there are a number of physical processes that can effectively reduce the cold gas content of galaxies in dense environments: (i) 'strangulation', i.e. the removal of the hot diffuse gas reservoir associated with galaxies falling into denser structures (Larson, Tinsley & Caldwell 1980); (ii) 'ram-pressure stripping' of cold gas suffered by galaxies travelling at large velocities through the diffuse intra-cluster medium (Gunn & Gott 1972); (iii) 'tidal stripping' due to the gravitational interaction with the parent halo or with other galaxies (Merritt 1983). (iv) 'galaxy harassment', i.e. the effect associated with repeated high-velocity encounters, which is believed to play a role in the formation of dwarf ellipticals or the destruction of low surface brightness galaxies in clusters (Moore et al. 1996). The efficiency of these processes at different scales has been studied extensively using detailed numerical simulations (e.g. Tonnesen & Bryan 2009; Tecce et al. 2010; Guo et al. 2011; Emerick et al. 2016; Steinhauser, Schindler

★ E-mail: lizhi.xie@inaf.it

& Springel 2016; Stevens et al. 2017). Their relative importance in driving the observed environmental trends remains, however, debated.

Recent studies have combined observational measurements with simulated accretion histories to constrain the time-scales for the suppression of star formation in satellite galaxies (related to the time-scale necessary to significantly deplete their cold gas reservoir). These are rather long (∼3–8 Gyr in the local Universe), with a dependence on both galaxy stellar mass and redshift (e.g. De Lucia et al. 2012; Wetzel et al. 2013; Hirschmann et al. 2014; Fossati et al. 2017). Although these results should be interpreted in a 'probabilistic' sense (not all galaxies will shut off simultaneously, and the scatter in quenching time-scale is likely correlated with the orbital distribution of infalling galaxies), these long time-scales are difficult to reproduce in theoretical models of galaxy formation (e.g. Hirschmann et al. 2014; Bahé & McCarthy 2015; Luo et al. 2016; Brown et al. 2017).

The ratio between the sizes of the star-forming and stellar discs ($R_{\rm SFR}/R_\star$) of satellite galaxies can provide important information about environmental processes: ram pressure is expected to remove first low-density gas at large distance from the galaxy centre. The stellar disc would be unaffected, at least until tidal stripping of stars becomes effective. Therefore, 'weak' ram-pressure stripping should cause a decrease of the H I size but would likely not affect significantly the molecular and stellar discs, leading to no significant evolution of the $R_{\rm SFR}/R_\star$ size ratio. 'Strong' ram-pressure stripping can affect the low-density H I and also the denser molecular gas in the disc, causing a decrease of the $R_{\rm SFR}/R_\star$ size ratio, up until the point at which the galaxy is completely quenched (i.e. no longer forms stars, even in the centre). In case of strangulation, the density of cold gas is expected to decrease at all radii, due to star formation and stellar feedback, so that the ratio between the sizes of the gaseous and stellar disc should remain approximately constant initially. The decreasing gas density leads to a lower molecular-to-atomic gas ratio and therefore a lower star formation efficiency, which becomes negligible at large radii. The shrinking star-forming region therefore leads to an increase of the size ratio between the HI and the stellar or molecular disc.

Statistical studies focusing on the size–mass relation have so far mainly focused on stellar disc sizes. These have indicated that late-type galaxies in dense environments are slightly more concentrated (have smaller sizes) than those in the field (Weinmann et al. 2009; Kuchner et al. 2017; Spindler & Wake 2017). Multi-wavelength surveys have allowed us to gather important information on how the gas content of individual galaxies is affected by the environment. Based on studies of galaxies in nearby clusters, Cortese et al. (2012) and Fossati et al. (2013) showed that H I-deficient galaxies have star-forming discs smaller than stellar discs, and that the size ratio decreases with HI deficiency. A large fraction of HI-deficient late-type galaxies are also depleted in molecular hydrogen, i.e. the star-forming reservoir (Boselli et al. 2002; Fumagalli et al. 2009). The depletion of H I is, however, more efficient than that of star-forming gas (Fabello et al. 2012; Catinella et al. 2013). Because of stripping galaxies in a dense environment can have truncated H I density profiles (Cayatte et al. 1990, 1994), molecular profiles (Fumagalli et al. 2009; Boselli et al. 2014b), dust profiles (Cortese et al. 2010), and Hα profiles (Kenney et al. 2004; Koopmann, Haynes & Catinella 2006; Fossati et al. 2013; Schaefer et al. 2017). In some cases, a tail of HI and ionized gas is observed (Gavazzi et al. 1995; Chung et al. 2009; Bellhouse et al. 2017; Jáchym et al. 2017), which can be interpreted as a consequence of ram pressure (Tonnesen & Bryan 2010).

Semi-analytic models of galaxy formation have been crucial to improve our understanding of the correlation between galaxy properties and their evolving environment. Xie et al. (2015) found that the size–mass relation of early-type central galaxies correlates tightly with the formation time of their host haloes: $R_\star \approx H(z(t_f))^{-2/3}$. On the basis of this result, we argued that the evolution of the stellar size, at fixed stellar mass, can be explained by differences in the halo assembly histories. These are expected to be large when comparing central and satellite galaxies: host haloes of satellite galaxies have likely formed earlier than those hosting central galaxies of the same stellar mass, and have suffered significant stripping after being accreted. In this work, we will combine observational estimates with state-of-the-art semi-analytic models to explore the origin of the observed size differences between centrals and satellite star-forming galaxies today.

This paper is organized as follows: Section 2 introduces the semi-analytic model used in this study and the observational samples considered. In Section 3, we compare observed and predicted integrated properties of central and satellite galaxies at $z = 0$, and explain the differences between centrals and satellites by studying their evolution histories. In Section 4, we review the prescriptions adopted to model disc sizes, and compare observational measurements and model predictions for the sizes of central and satellite galaxies. In Section 5, we discuss our results and then summarize them in Section 6.

2 THE GALAXY FORMATION MODEL AND OBSERVATIONAL DATA

In this section, we introduce the model and the observations that we use in this paper, and discuss how we select model galaxies to be compared with data.

2.1 The galaxy formation model

In this work, we take advantage of the latest version of our GAlaxy Evolution and Assembly (GAEA) model. GAEA features a sophisticated chemical enrichment scheme (De Lucia et al. 2014) that accounts for the non-instantaneous recycling of gas, metals and energy from massive stars and different types of supernovae, and a new stellar feedback scheme based partly on results from hydrodynamical simulations (Hirschmann, De Lucia & Fontanot 2016). The version of GAEA we use in this work also includes an explicit treatment for the partition of cold gas in molecular (H_2) and atomic hydrogen (HI), and H_2-based star formation laws (Xie et al. 2017). Specifically, we use here the prescriptions based on the empirical relation by Blitz & Rosolowsky (2006, BR06 in Xie et al. 2017), as this model provides a better agreement with different observational data, including the $M_{\rm H\,I} - M\star$, $M_{\rm H_2}$–$M_\star$ scaling relations and the H I and H_2 mass functions measured in the local Universe.

For the present analysis, we apply our model to the Millennium II simulation (MSII; Boylan-Kolchin et al. 2009). This corresponds to a box of 100 Mpc h^{-1}, simulated employing a particle mass of 6.89×10^6 $M_\odot$ h^{-1}. The simulation assumes a *WMAP*1 cosmology, with $\Omega_{\rm m} = 0.25$, $\Omega_{\rm b} = 0.045$, $\Omega_\Lambda = 0.75$, $h = 0.73$, and $\sigma_8 = 0.9$. More recent measurements from e.g. *PLANCK* (Planck Collaboration et al. 2015) and *WMAP*9 (Bennett et al. 2013) provide slightly different cosmological parameters and, in particular, a larger value for $\Omega_{\rm m}$ and a lower one for σ_8. As shown in previous work, however, these differences are expected to have little influence on model predictions, once the parameters are retuned to reproduce a given set of observables in the local Universe (Wang et al. 2008; Guo et al.

2013). As discussed in Xie et al. (2017) and in our previous work, our model applied to the MSII can resolve well galaxies with stellar mass $M_\star > 10^8\,\mathrm{M}_\odot$.

For the following discussion, it is worth noting that our model assumes that the hot gas associated with galaxies infalling on larger systems (i.e. becoming satellites) is instantaneously stripped. Satellite galaxies can continue forming stars until their reservoir of cold gas is exhausted. Finally, we do not include a modelling for the stripping of cold gas due to ram pressure (Gunn & Gott 1972).

From the model, we randomly select 6000 'star-forming' satellite galaxies. These are selected by fitting the predicted SFR–stellar mass relation for satellites (we find: $\log SFR_{\mathrm{MS,\,m}} = 0.9\log M_\star - 8.8$), and then considering only galaxies with $\log \mathrm{SFR} > \log \mathrm{SFR}_{\mathrm{MS,\,m}} - 1$. For each of these satellite galaxies, we also select a central star-forming galaxy (using the same 'star-forming' definition) among those with V_{max} comparable to the halo V_{max} of the satellite galaxy at the time it was accreted (i.e. at the last time it was a central galaxy). Specifically, we require $-0.1 < \delta\log V_{\mathrm{max,\,acc}} < 0.5$,[1] where $\delta\log V_{\mathrm{max,\,acc}}$ is the difference between the halo V_{max} of the central and satellite galaxies at the satellite's accretion time. Since in our model we keep V_{max} fixed to the value the satellite galaxy had at the last time the galaxy was central, this allows us to match centrals and satellites that were in similar 'environments' before environmental effects start playing a role.

The selected sample is representative of star-forming satellites. These have been accreted between $z \sim 1$ and $z \sim 0.02$ and, at present, they reside in haloes with mass ranging between 10^{10} and $3 \times 10^{14}\,\mathrm{M}_\odot$ with median $\sim 10^{13}\,\mathrm{M}_\odot$. Their central counterparts are typically hosted by lower mass haloes (ranging between 10^{10} and $3 \times 10^{14}\,\mathrm{M}_\odot$, with median halo mass $\sim 2 \times 10^{11}\,\mathrm{M}_\odot$.) depending on the stellar mass.[2]

2.2 Observational data

In this work, we use data from the *Herschel* Reference Survey (HRS – Boselli et al. 2010), the extended *GALEX* Arecibo SDSS Survey (xGASS – Catinella et al. 2018) and from the Hα Galaxy Groups Imaging Survey (HAGGIS – Kulkarni et al. 2014).

HRS is a volume-limited, *K*-band-selected sample of 322 local galaxies (15<dist<25 Mpc), including fairly isolated objects and galaxies within the Virgo cluster. In this paper, we focus on late-type star-forming galaxies and exclude 22 galaxies that are classified as elliptical galaxies. The stellar mass is calculated from *i*-band luminosity and $g - i$ colour (Zibetti, Charlot & Rix 2009; Cortese et al. 2012). The star formation rates (SFRs) used in this paper are obtained by averaging four different estimates by Boselli et al. (2015) and correcting for dust attenuation. The HRS also includes atomic hydrogen masses from ALFALFA (Giovanelli et al. 2005; Haynes et al. 2011) and Springob et al. (2005) and molecular hydrogen mass (Boselli, Cortese & Boquien 2014a). The latter are obtained from CO(1–0) luminosity using a constant conversion factor $X_{\mathrm{CO}} = 2/3 \times 10^{20}\,\mathrm{cm}^{-2}/(\mathrm{K\,(km\,s^{-1})})$. The effective radii of the star-forming and stellar components of each galaxy corresponds to the half-light radii of the Hα emission and in the *r* band, respectively. We exclude 68 galaxies with no information of sizes or SFR. This selection leaves us with 233 galaxies, including 54 in the core of the Virgo cluster, 59 falling on to the cluster and 120 non-Virgo galaxies (Gavazzi et al. 1999). We consider galaxies in the cluster core and those infalling as 'satellites', and those non-Virgo galaxies as 'centrals' (this might include some non-Virgo satellite galaxies in the sample of central galaxies.).

HAGGIS is a narrow band Hα imaging survey that includes 390 galaxies located in over 100 galaxy groups with halo mass ranging between 10^{12} and $10^{14}\,\mathrm{M}_\odot$. These have been selected from the Sloan Digital Sky Survey (SDSS) group catalogue by Yang et al. (2007). Galaxies are classified as centrals or satellites based on the original Yang et al. classification. The *i*-band luminosities are also based on SDSS data. The stellar masses of HAGGIS galaxies are estimated from the $g - i$ colour and *i*-band luminosity as for the HRS galaxies. The SFR is estimated from the extinction-corrected Hα luminosity. HAGGIS does not provide information for gas masses, and includes both star-forming and quiescent galaxies. For our analysis, we exclude galaxies with no detection in Hα and no assignment of halo mass. AGN galaxies are also excluded from HAGGIS for the inaccurate estimating on their SFRs and SFR radii.

xGASS is a gas fraction-limited census of 1179 galaxies in the local Universe ranging between $10^9 < M_\star$ and $10^{11.5}\,\mathrm{M}_\odot$. The HI detections are from GASS (Catinella et al. 2013), GASS-low (Catinella et al. 2018), and ALFALFA (Haynes et al. 2011). We use only the non-confused H I-detected galaxies. Each galaxy is classified as a central or a satellite based on the SDSS group catalogue by Yang et al. (2007). The stellar mass is taken from the SDSS MPA/JHU catalogue. The SFR is estimated from the ultra-violet (UV; from *GALEX* – Martin et al. 2005; Morrissey et al. 2007) and mid-infrared (MIR) luminosity (*from Wide-field Infrared Survey Explorer* -- Wright et al. 2010), or SED fitting (Wang et al. 2011). xCOLDGASS (Saintonge et al. 2017) provides CO detections for 290 galaxies and upper limits for 122 galaxies. We convert the CO(1–0) luminosity to H_2 mass using a constant conversion factor as done for HRS galaxies. xGASS provides half mass radii based on *r*-band imaging, but no information for the SFR radii. Therefore, we do not include xGASS in our analysis of galaxy sizes.

All properties of observed galaxies are corrected to a Chabrier IMF and *WMAP* 1 yr cosmology as used in our galaxy formation model.

In Fig. 1, we plot the distribution of integrated properties for all galaxies from the HRS (red squares), xGASS (green dots), HAGGIS (blue crosses), and all model galaxies (black contours) at $z = 0$. Most of the HRS galaxies have stellar masses below $\sim 10^{10}\,\mathrm{M}_\odot$, while xGASS and HAGGIS include relatively more massive galaxies. Measurements from the different surveys are consistent with each other, and our model reproduces the observed distributions relatively well, both for centrals and for satellite galaxies.

The top and middle panels show the H I mass and H_2 mass as a function of galaxy stellar mass. Model galaxies follow the same distribution as galaxies from HRS and xGASS on the H I mass–stellar mass plane. The middle panels show, instead, that the model slightly overpredicts the H_2 masses of central galaxies and slightly underpredicts the H_2 masses of satellites. The bottom panels show the relation between SFR and stellar mass. HRS and xGASS include more galaxies with high SFR than HAGGIS. Model galaxies occupy the same region of data for both central and satellite galaxies when compared to galaxies from HRS, but predict a narrower distribution at large stellar masses with respect to galaxies from xGASS and

[1] An asymmetric range is used because of the non-uniform distribution of halo masses.

[2] The satellite population selected from the model follows a similar distribution of halo masses as satellite galaxies from the HAGGIS and the xGASS. Satellites in the HRS are located in the Virgo cluster. For central galaxies, model galaxies are hosted on average by lower mass haloes than those in observations.

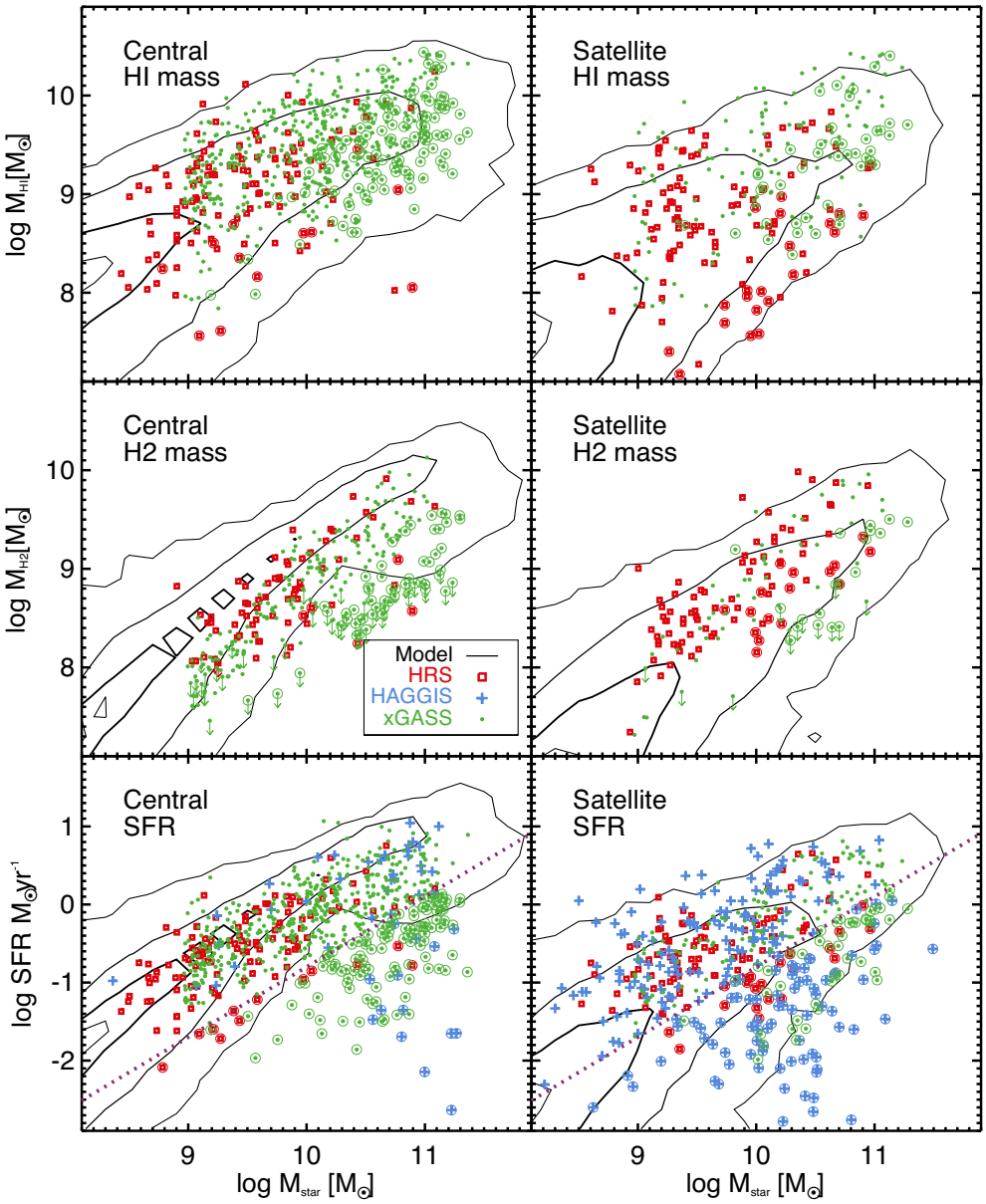

Figure 1. Distributions of H I mass (top), H_2 mass (middle) and SFR (bottom) for central (left) and satellite (right) galaxies as a function of stellar mass. The black contours show the number density of all central/satellite galaxies in the model, with thin to thick lines indicating number densities corresponding to 1, 10, 50 per cent of the peak density. The red squares, green dots and blue crosses represent galaxies from HRS, xGASS and HAGGIS, respectively. Symbols with open circles represent passive galaxies that are more than 1 dex below the main sequence. Symbols with downwards arrows are upper limits. The purple dotted line in the bottom panels shows the SFR cut adopted to select star-forming galaxies from the data and the model.

HAGGIS. We select star-forming galaxies from the data using the same SFR cut as the one used for model galaxies (shown as a purple dotted line in bottom panels of Fig. 1). We have tested lower SFR cuts and also a different (empirical) MS relation (Speagle et al. 2014) to select star-forming galaxies. We find that our results are not affected by these different choices qualitatively.

3 INTEGRATED PROPERTIES OF CENTRAL AND SATELLITE GALAXIES

In this section, we analyse the differences between integrated properties of central and satellite galaxies, and compare our model predictions with observational data.

3.1 Differences at present time

Fig. 2 shows the median scaling relations of central (left column) and satellite (middle column) star-forming galaxies. The black lines show the median and standard deviation of the distributions predicted by our model. The coloured symbols are running medians computed from the observational samples. Specifically, we have sorted the galaxies in the samples by their stellar mass, and computed the median properties and standard deviations in bins containing nine galaxies.[3] Our model reproduces reasonably well the

[3]Changing the number of galaxies in the calculation of the running median, or in the estimation of the difference between centrals and satellites described later in the text, does not affect our results qualitatively.

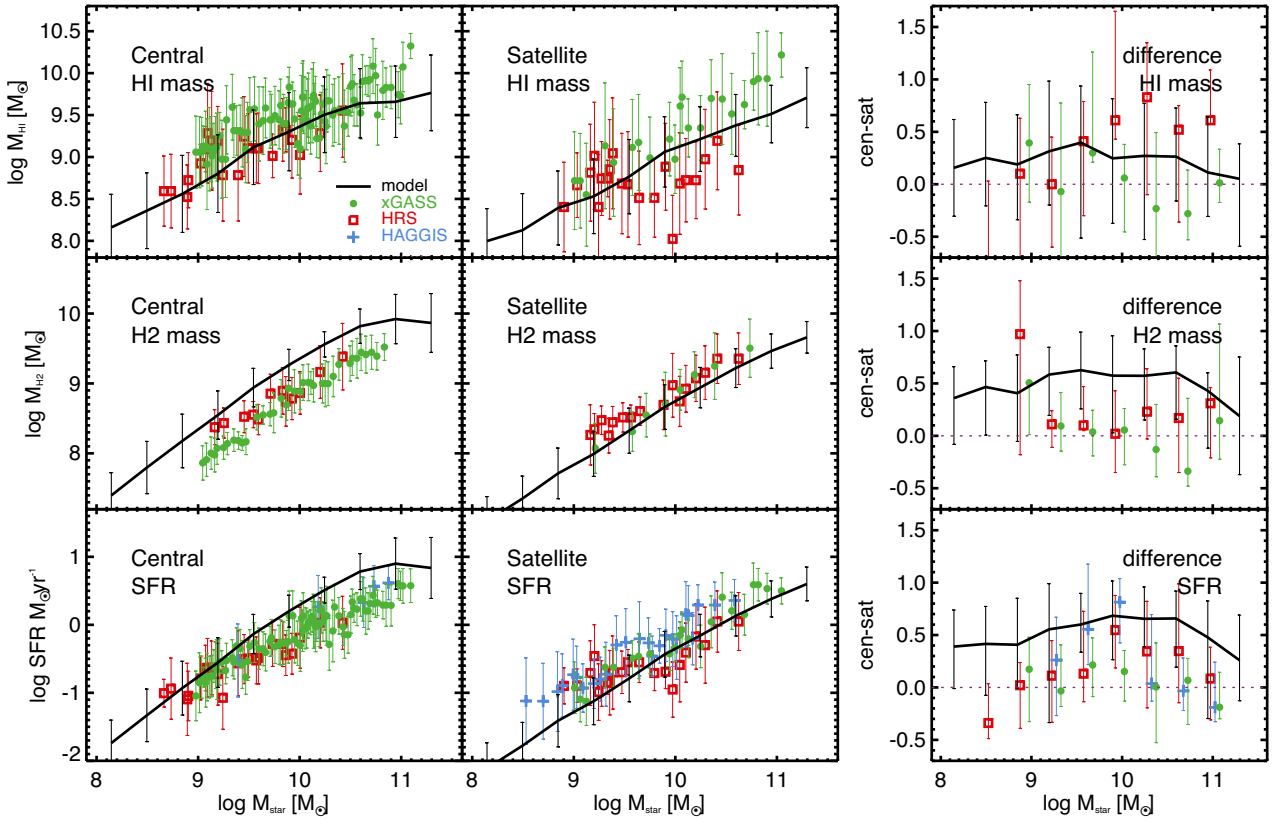

Figure 2. The top, middle, and bottom rows show the median H I mass, H_2 mass, and SFR as a function of galaxy stellar mass for centrals (left column) and satellites (middle column). The right column shows the differences between the integrated properties of central and satellite galaxies. Red squares, blue crosses, and green dots show the data from HRS, HAGGIS and xGASS, respectively. The solid black lines show our model predictions. In the left and middle columns, black lines and error bars correspond to median values and standard deviations, while coloured symbols are running medians with a window width of nine galaxies. In the right column, black lines and coloured symbols show median differences and error bars the 9th and 98th percentiles (more details in the text). The purple line is shown as a reference.

distribution observed for H I masses of both central and satellite galaxies. For the molecular gas content and the SFR, the agreement is less good. Specifically, the model overpredicts by 0.3 dex the H_2 mass of central galaxies, and underestimates by ∼0.1 dex that of satellites galaxies. In addition, the model predicts a steeper SFR–$M_\star$ relation than observed, which is a common problem for semi-analytic models [e.g. see discussions in Xie et al. (2017); Cora et al. (2018)]. In order to account for inconsistencies between model predictions and observational measurements for central galaxies, and focus on environmental effects, we concentrate below on the differences between centrals and satellites.

The right column shows the differences between central and satellite galaxies. To estimate the uncertainty of these differences, we randomly select nine galaxies in a given stellar mass bin from the central and satellite samples, and compute the difference between the median values of each sub-samples. Results change significantly by repeating the procedure. In order to give a conservative estimate of the scatter, we repeat the selection 50 times and show as error bars the 2nd and 98th percentiles of the distributions of the estimated differences. We find that, both for our model galaxies and for the observational samples, star-forming satellite galaxies have less gas and lower SFR than central galaxies of similar stellar mass. Specifically, we find that the model central–satellite difference is ∼0.2 dex for the HI mass and more than a factor of 2 larger (∼0.5 dex) for the H_2 mass and the SFR. The central–satellite differences for the observed galaxies show a larger variation. The xGASS and HRS are roughly consistent with each other and give a central–satellite difference for the HI mass that is comparable to that predicted. The differences measured for the H_2 mass and SFR are instead smaller (<0.2 dex) than those predicted by our model. The consistency between model predictions and observational estimates is worse if a lower SFR selection cut is adopted. This is due to a more rapid depletion of the molecular gas content (and therefore a more rapid suppression of the SFR) in the model with respect to the data. As discussed in the Introduction, this is a problem shared by most existing theoretical models of galaxy formation (see e.g. Hirschmann et al. 2014; Brown et al. 2017). We will further discuss possible solutions to this problem in Section 5.

3.2 Evolution of the difference between central and satellite galaxy

We then take advantage of our model results to understand how and when the differences between centrals and satellites measured today are established. To this aim, we compare the properties of galaxies at fixed halo $V_{\rm max,\,acc}$, i.e. at fixed values of $V_{\rm max}$ at the accretion time of the satellite galaxies. We assume that $V_{\rm max,\,acc}$ is representative of the 'environment' of the galaxy at accretion time, so that centrals and satellites in haloes with similar $V_{\rm max,\,acc}$ are assumed to have evolved in similar environments before accretion.

Since we have selected centrals by matching their $V_{\rm max,\,acc}$ with that of the satellites at the time of accretion, the stellar mass of satel-

lite galaxies will be, in general, different from that of their central counterparts. Specifically, we find that the difference in stellar mass ranges from 0.6 to −0.4 dex for galaxies in haloes from low $V_{\rm max.acc}$ to high $V_{\rm max.acc}$. To remove the dominant trend with galaxy stellar mass, we compare the difference between 'normalized' properties: Fig. 2 shows that the scaling relations for H I mass, H_2 mass, and SFR for model galaxies are well fitted by $M_{\rm H\,I} \propto M_\star^{0.6}$, $M_{\rm H2} \propto M_\star^{0.9}$, and SFR $\propto M_\star^{0.9}$. We assume the slopes of these relations do not vary with cosmic time and normalize the H I mass, H_2 mass, and SFR by $M_\star^{0.6}$, $M_\star^{0.9}$, and $M_\star^{0.9}$, respectively.

The top left panel of Fig. 3 shows the differences between the normalized HI mass of central and satellite galaxies at accretion time (green dashed) and now (solid black). At present time, central galaxies have 0.2 dex more H I than their satellite counterparts (this is similar to the difference shown in Fig. 2 when comparing central and satellite galaxies at fixed stellar mass.). The difference at accretion time ranges from −0.1 to −0.3 dex. Therefore, the difference between normalized HI mass of central and satellite galaxies has increased by about 0.3–0.4 dex since accretion.

The evolution of the central–satellite difference is explained by the bottom left panel, showing the difference between the normalized H I mass for centrals (solid blue lines) and satellites (red dashed lines) predicted at present and at the time of accretion. For central galaxies, the normalized H I mass remains unchanged since accretion. For satellite galaxies, the normalized HI mass decreases by up to 0.4 dex, with a mild dependence on the $V_{\rm max,\,acc}$. The reason for this differential evolution is that satellite galaxies lose H I due to environmental effects (stripping of the hot gas reservoir in our case). The trend with $V_{\rm max,\,acc}$ can be explained by the fact that satellites accreted in more massive haloes have been accreted on average earlier than satellites in lower mass haloes, and therefore there was more time to deplete their cold gas reservoir

The middle and right columns show results for the normalized H_2 mass and SFR. At present time, the difference of both H_2 normalized mass and normalized SFR at fixed $V_{\rm ,\,max,\,acc}$ is about 0.3−0.4 dex. At accretion time, the difference varies between −0.2 dex and zero. After accretion, the difference has increased by ∼0.5 dex. The bottom panels show the differences between normalized H_2 mass/SFR of galaxies at present and accretion time. Central galaxies (blue solid lines) lose ∼0.2 dex of their normalized H_2 mass and SFR since accretion, which corresponds to the redshift evolution of H_2 mass–stellar mass relation and SFR–stellar mass relation. For satellite galaxies (red dashed lines), the decrease of both H_2 normalized mass and normalized SFR is more pronounced, particularly for haloes that are more massive at the time of accretion: the decrease is up to 0.8 dex in the $V_{\rm max,\,acc}$ range we have considered.

To summarize, the model and observational data predict consistent trends for satellite galaxies with small difference in the amplitude. The model predicts that central and satellite galaxies which evolved in similar environment before accretion have slightly different integrated gas properties. Specifically, central galaxies have slightly less H I mass, H_2 mass, and lower SFR than satellite galaxies on average. As we have discussed, the difference between integrated properties of centrals and satellites observed at $z = 0$ can be ascribed to environmental effects.

4 DIFFERENCE IN SIZES OF GASEOUS AND STELLAR DISCS

In this section, we focus on the sizes of gaseous and stellar discs. We discuss how disc sizes and angular momenta of central and satellite star-forming galaxies evolve in the framework of our semi-analytic model, and how the predicted differences between central and satellite galaxies compare to observational measurements. We then trace the evolution of our model galaxies to determine when such differences arise and why.

4.1 Disc sizes and angular momentum evolution in the model

Galaxies sizes are modelled by tracing the angular momentum of the gaseous and stellar components, as described in Guo et al. (2011). We assume that gaseous and stellar discs are rotationally supported, in equilibrium, and described by exponential density profiles. Under these assumptions, their scalelengths are given by (Mo, Mao & White 1998):

$$r_{\rm gas,d} = \frac{J_{\rm gas}/M_{\rm gas}}{2V_{\rm max}}, \quad r_{\star,\rm d} = \frac{J_\star/M_\star}{2V_{\rm max}}, \tag{1}$$

where $J_{\rm gas}$, and $J_\star$ are the angular momenta of the gaseous and stellar disc, respectively. $M_{\rm gas}$, and $M_\star$ are the total mass of gas and stars in the disc. $V_{\rm max}$ is the maximum circular velocity and is computed from the actual distribution of dark matter particles in the haloes associated with model galaxies. In the case of satellite galaxies, this quantity corresponds to that of the parent halo at the last time the galaxy was central.

The stellar and gaseous discs of galaxies gain mass and angular momentum through various physical processes. We assume that the specific angular momentum of the hot gas (i.e. the diffuse baryons that are shock heated during accretion on to the dark matter halo) is identical to that of the host dark matter halo. Recent work based on hydro-dynamical simulations (e.g. Stevens et al. 2017; Danovich et al. 2015) has shown that the gas accreted through the 'rapid cooling regime' (effective at high redshift and in small haloes) can carry an angular momentum from two to four times larger than that of the parent dark matter halo. In Zoldan et al. (2018), we show that this does not significantly influence the size of late-type model galaxies in the local Universe.

The gaseous disc then gains or loses angular momentum and mass through: (i) gas cooling, that transfers gas from the hot halo to the cold gas disc; (ii) star formation, that turns a fraction of the cold gas into stars; (iii) recycling, that turns a fraction of the stars back into cold gas; (iv) supernovae feedback, that heats a fraction of the cold gas up to the virial temperature of the halo, and ejects a fraction of the heated gas out into the inter-galactic medium; (v) mergers, that bring gas from satellite galaxies on to centrals[4] and can convert (depending on the mass ratio) part of the remnant gas into stars. The same physical processes, with the exclusion of gas cooling and supernovae feedback, affect the angular momentum of the stellar disc. In addition, this component is affected by disc instabilities. This process moves some stars from the inner disc to a non-rotational bulge, which decreases the mass of the stellar disc while conserving its angular momentum. Therefore, in our models, disc instability events increase the specific angular momentum and size of the stellar disc.

The variations of angular momentum for the gaseous ($\Delta \boldsymbol{J}_{\rm gas}$) and stellar ($\Delta \boldsymbol{J}_\star$) disc at each code time-step can be written as:

$$\Delta \boldsymbol{J}_{\rm gas} = \boldsymbol{J}_{\rm cooling} - \boldsymbol{J}_{\rm SF} + \boldsymbol{J}_{\rm recycling} + \boldsymbol{J}_{\rm merger,gas} - \boldsymbol{J}_{\rm SNfb}, \tag{2}$$

[4]Our model also includes satellite—satellite mergers, i.e. mergers between 'orphan' galaxies and satellite galaxies still associated with a distinct dark matter substructure. These are, however, rare.

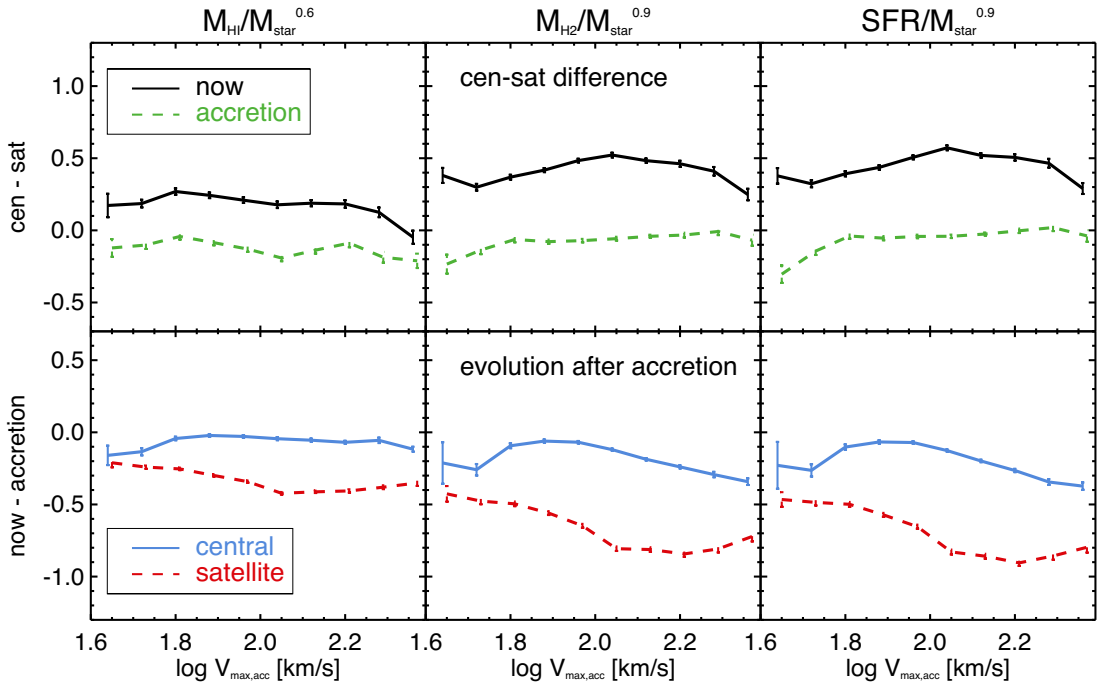

Figure 3. Top panels show the differences between the normalized H I mass (left column), H_2 mass (middle column), and SFR (right column) of centrals and satellites predicted at present (solid black lines) and at the time of accretion (green dashed lines). The bottom quantities show instead the difference between properties predicted at present and at the time of accretion. Solid (blue) and dashed (red) lines are used for central and satellite galaxies, respectively. Lines correspond to the median of the distributions while error bars show the errors on the mean.

and

$$\Delta \boldsymbol{J}_\star = \boldsymbol{J}_{\rm SF} - \boldsymbol{J}_{\rm recycling} + \boldsymbol{J}_{\rm merger,\star} + \boldsymbol{J}_{\rm inst}. \quad (3)$$

In the following, we define the size of the gaseous disc as that enclosing half of the total gas mass and the size of the stellar component as the radius enclosing half of the stars in the bulge+disc. The stars and the gas in the disc are assumed to follow an exponential distribution with scalelength given by equation (1), while those in the bulge are assumed to be distributed according to a Jaffe (1983) profile.

We partition the gaseous disc in an HI and an H2 component, and form stars only from the latter. As explained in detail in Xie et al. (2017), the partition is performed in 21 annuli, which allows us to compute the extent of the star-forming region. In the following, we define the SF size as the radius enclosing half of the total SFR for each model galaxy. In our model, the distribution of the newly formed stars follows that of the entire gaseous disc (HI+H2) at the time of the star formation, but the amount of stars formed depends on the estimated molecular-to-atomic gas ratio. Eliminating this inconsistency requires a more realistic treatment of angular momentum exchanges, which accounts for the multi-phase nature of the cold gaseous disc. This goes beyond the aims of this work, and we plan to address this problem in future work.

4.2 Contribution to disc growth from different physical processes

In Fig. 4, we show the growth of the gaseous and stellar disc radii for two example galaxies (a central galaxy in the top panels, and a satellite galaxy in the bottom ones). These have been randomly selected among model galaxies with stellar bulge-to-total mass ratio smaller than 0.3, and stellar mass $M_\star \sim 10^{10}\,{\rm M}_\odot$. The left panels show the evolution of the gaseous disc scalelength as a function of the gas mass. Each segment corresponds to a change in disc scalelength and/or gas mass, and is colour-coded according to the physical processes that have driven that variation. The middle panels show the corresponding evolution in the size–mass plane for the stellar component of the disc.[5] The figure shows that the gas disc mainly evolves (both in mass and in size) through gas cooling. The gas disc size can increase or decrease due to cooling depending on the instantaneous value of the dark matter halo spin. Stellar feedback decreases the cold gas mass (moving a fraction of it into the hot gas reservoir), but it does not affect the size of the disc because the specific angular momentum of the gas is conserved. Therefore, time-steps during which the evolution is driven by supernovae feedback are shown as horizontal green lines. Recycling does not affect significantly the mass of the disc, but it can significantly modify its size adding back into the inter-stellar medium gas with lower specific angular momentum from previous stellar populations. This is particularly notable at early times, so that blue segments (showing time intervals during which the evolution is driven by recycling) at early times are almost vertical. At later times, the variation in mass due to recycling becomes more significant than the variation it causes in size. The bottom left panel shows that, before accretion on to a more massive system (this is marked by a black circle), the size evolution of satellite galaxies follows similar trends as for central galaxies. After accretion, the gas disc loses mass because of star formation and stellar feedback, and gains mass through gas

[5] As explained in the previous section, the stellar size includes the bulge. So, strictly speaking, we are looking here at the stellar component of the entire galaxy, and not of the disc. However, these galaxies are selected to be disc-dominated so that the stellar size of the disc is generally very close to that of the galaxy.

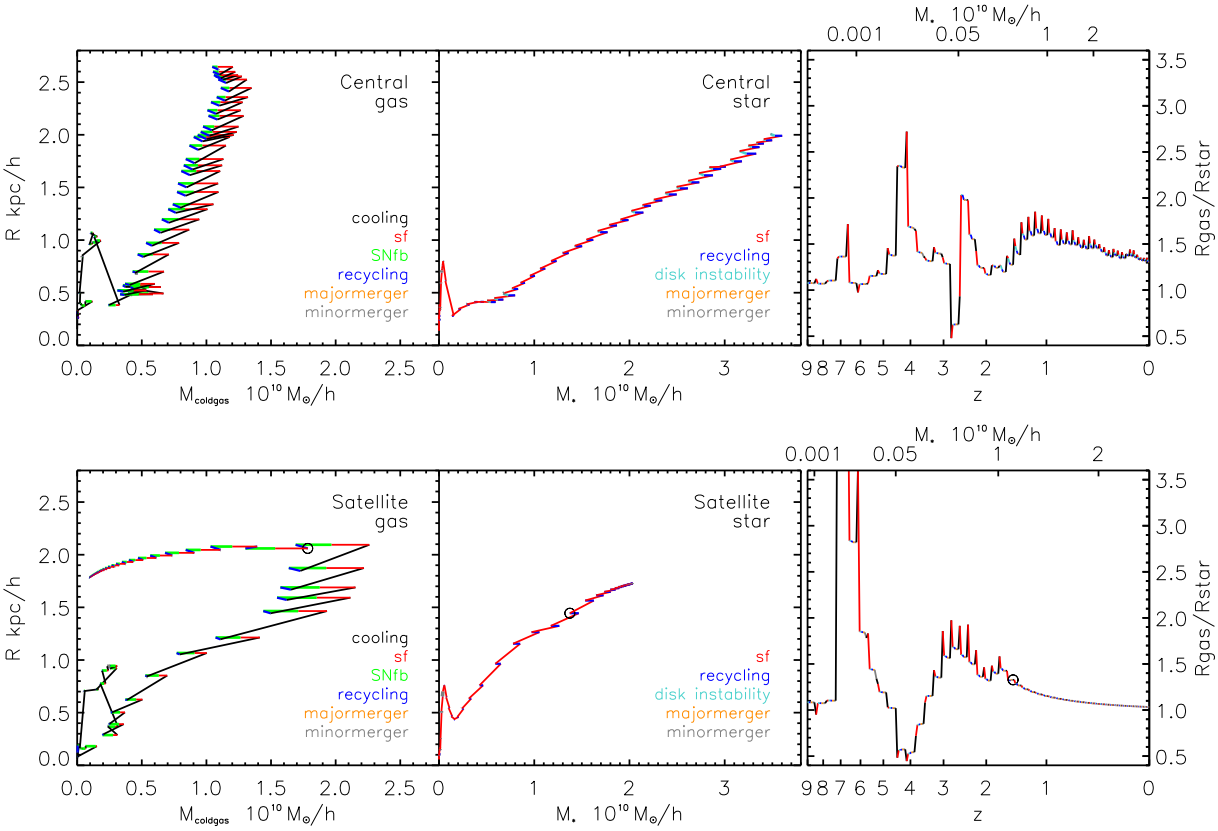

Figure 4. The growth of two example galaxies in the size–mass plane. The top panels correspond to a disc-dominated central galaxy, while the bottom panels correspond to a satellite galaxy. The left (middle) panels show the evolution of the scalelength of the gaseous (stellar) disc as a function of the gas (stellar) mass. The insets show a zoom in on the late time evolution. The grey circle in the bottom panels marks the accretion time for the satellite galaxy (i.e. the time corresponding to the last time the galaxy is central). The right panels show how the ratio between the scale radius of the gaseous and stellar disc evolves as a function of redshift. In all panels, coloured lines show variations of the quantities shown corresponding to different physical processes (as labelled), and occurring at each code time-step. Grey thin curves in the right panels connect size ratios measured at subsequent snapshots.

recycling. Since there is no additional gas cooling, and only relatively small fractions of stars are formed after accretion, the specific angular momenta of the gas and stellar discs (and therefore their sizes) are not significantly modified after accretion.

The middle panels of Fig. 4 show the evolution of the stellar disc size as a function of the stellar disc mass. The evolution of the stellar disc size generally follows that of the corresponding gaseous disc, with the evolution being driven primarily by star formation. What happens, typically, is that the gaseous disc grows first due to cooling. Star formation then transfers the angular momentum of the gas to the stellar component, driving the growth of the stellar disc. This is displayed nicely in the right panels, which show how the ratio between the scalelength of the gaseous disc and that of the stellar disc varies as a function of redshift. The size ratio oscillates significantly, with gas cooling generally leading to an increase of the gaseous disc size (and therefore an increase in the size ratio plotted), and star formation increasing the size of the stellar disc (therefore decreasing the size ratio). For the satellite galaxy examined, the size of the stellar disc keeps growing (although very little) after accretion, and the final size ratio is slightly larger than unity.

Fig. 5 summarizes the fractional contribution of various physical processes to the growth of the gaseous (left column) and stellar (right column) disc sizes. Top and bottom panels correspond to central and satellite galaxies, respectively. The quantities plotted have been computed averaging results for late-type ($B/T < 0.3$) galaxies. Let us focus first on the top panels (central galaxies): the figure confirms that, on average, cooling drives the growth of the gaseous disc size, with a trend for an increasing contribution with increasing stellar mass. The contribution from major mergers is negligible, which is not surprising given these galaxies have been selected to be disc dominated. The contribution from minor mergers is also very small, but somewhat more important for galaxies more massive than $\sim 10^{11}$ $M_{\odot}$. Recycling on average gives a negative contribution to gas disc growth, i.e. it tends to decrease the size of the gaseous disc because it typically restitutes gas of lower specific angular momentum. The stellar disc of central galaxies grows ∼90 per cent of its size through star formation. This fraction is constant over the stellar mass range considered. Minor mergers contribute for less than 10 per cent of the stellar disc growth size, for all galaxy stellar masses considered. Finally, disc instability contributes very little for low-mass galaxies and is somewhat more important (the contribution is never higher than 10 per cent) for more massive galaxies.

The bottom panels of Fig. 5 show the corresponding fractional contributions from different physical processes for satellite galaxies. In this case, lines with symbols show the contribution to size growth by different physical processes after accretion ($z \sim 0.45$ on average). The results are consistent with contributions for central galaxies, indicating that there is no obvious difference in size evolution between central and satellite galaxies in our model. After

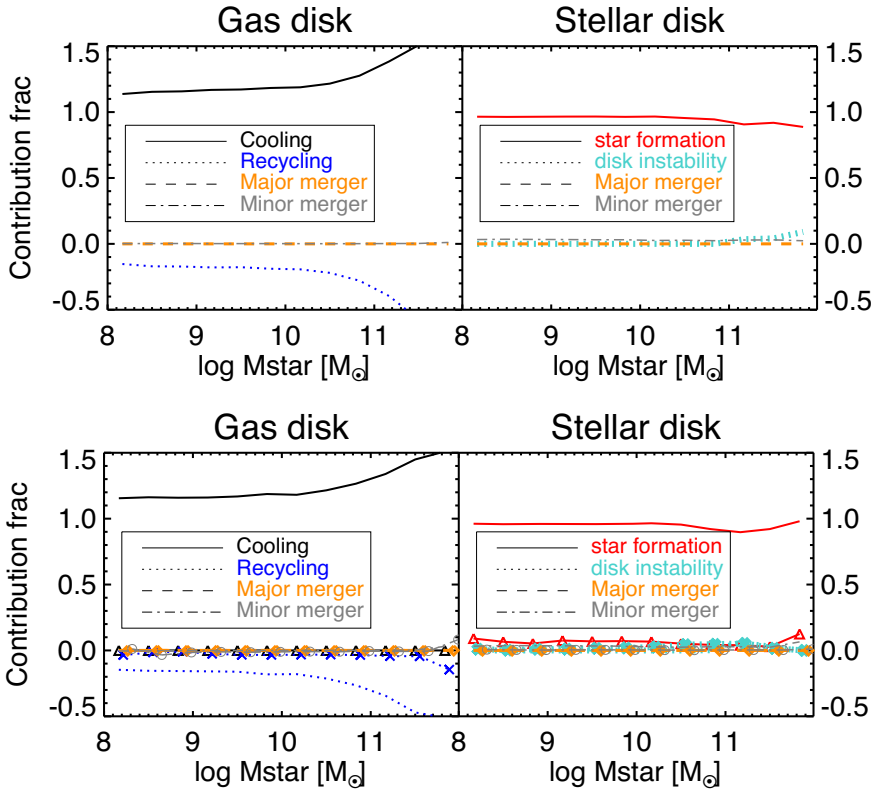

Figure 5. Median fractional contribution of different physical processes in determining the final sizes of gas discs and stellar discs, as a function of the galaxy stellar mass. Top and bottom panels show results for central and satellite galaxies, respectively. In the bottom panels, dashed lines correspond to the contributions by different physical processes after accretion. Only disc-dominated galaxies have been included in the analysis ($B/T < 0.3$).

accretion, both gaseous and stellar sizes grow very little. In particular, stellar sizes grow due to star formation while the gaseous disc sizes tend to decrease slightly due to gas recycling (and minor mergers).

4.3 Differences of radii between central and satellite galaxies

We compare the stellar and SF radii of model galaxies with observational measurements in Fig. 6. Top and bottom rows show the distribution of SF and stellar radii, respectively, as a function of the galaxy stellar mass. Left and right columns show results for central and satellite galaxies. Red squares and blue crosses represent individual galaxies from HRS and HAGGIS (we have included quiescent galaxies, marked with open circles, in this case.). These two data sets exhibit consistent distributions for the SF and stellar sizes, with HAGGIS including a larger fraction of galaxies with low SFR at the massive end, which leads to a larger scatter in the distributions. The black contours show the distribution of all model galaxies. These occupy the same region of observed galaxies and exhibit a similar scatter.

We then select star-forming galaxies from the model and the observational samples, and compare their median radii at fixed stellar mass in Fig. 7. In the top panels, the median SF sizes of observed galaxies lie between median values predicted for the SF radii and the gaseous disc radii of model galaxies. Median stellar radii of model galaxies are in reasonable agreement with observational measurements. In the right column, we plot the differences between central and satellite galaxies against stellar mass. These differences have been calculated following the same procedure described for Fig. 2. We find that model central galaxies have ∼0.1 dex larger SF radii than model satellite galaxies at fixed stellar mass. A similar difference is found for galaxies in HRS and HAGGIS, although the scatter is very large. We also plot the differences for the model gaseous disc sizes as dotted lines in the top panels, and find that these are only slightly smaller than the difference we predict for SF sizes. Both in the model and in the data, central and satellite galaxies have similar stellar radii at fixed stellar mass (bottom right panel).

As done for the integrated properties, we then analyse the evolution of central and satellite galaxies, and compare the central–satellite differences at the accretion time and now. In order to remove trends with galaxy stellar mass, we normalize the sizes by $M_\star^{0.2}$. Indeed, Fig. 7 shows that the relation between SF, gas or stellar radii and stellar mass is well fitted by a power law with index 0.2.

Top left panel of Fig. 8 shows the differences between the normalized SF radii of satellite galaxies and those of their central counterparts. At present time, the SF radii of central galaxies are about ∼0.1 dex larger than those of their satellite counterparts. Differences are smaller for the gaseous disc radii. At the time of accretion, central galaxies have smaller SF radii than their satellite counterparts, with a difference ranging between -0.1 and 0.03 dex. Comparable differences are found for the gaseous disc radii. The difference between the SF radii of central and satellite galaxies has increased by 0.1 dex since accretion time. For the gaseous disc radii (green dot–dashed line and black dotted line in the top-left panel) the difference between centrals and satellites has increased by a smaller amount. The bottom left panel shows the evolution

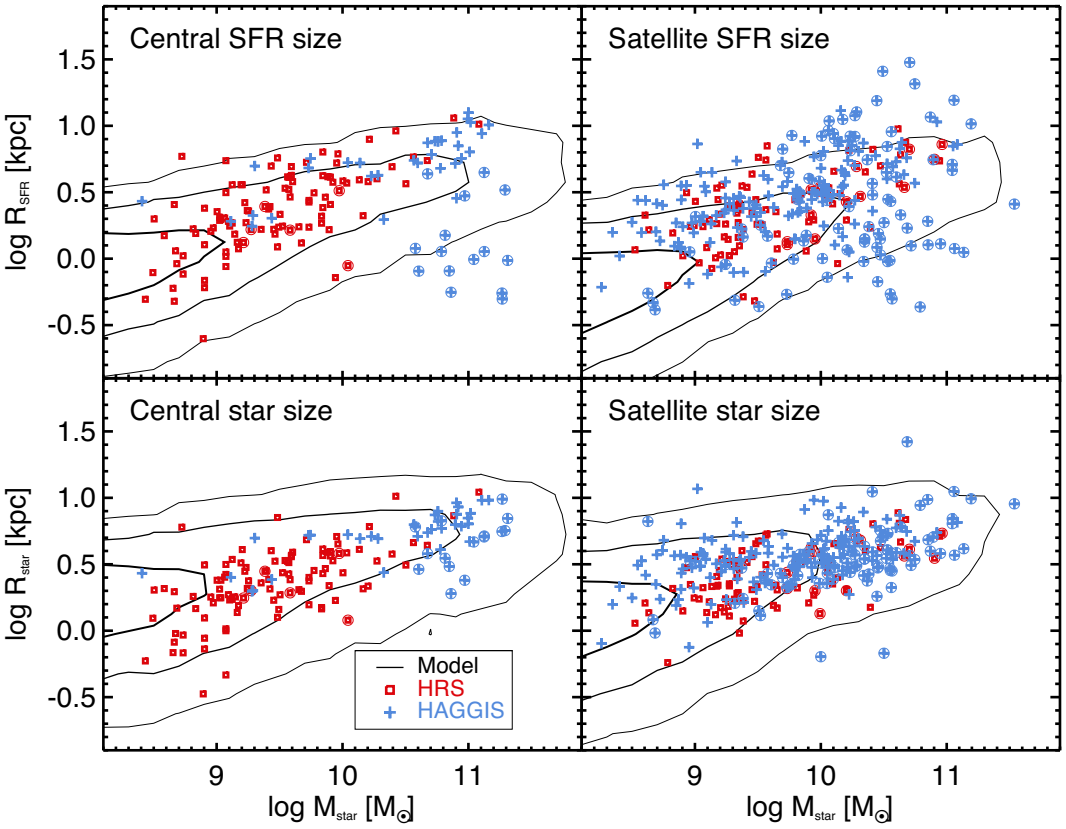

Figure 6. Distributions of the size of the star-forming region (top), stellar size (middle) and gas size (bottom) for central (left) and satellite (right) galaxies as a function of stellar mass. Symbols and contours have the same meaning as in Fig. 1.

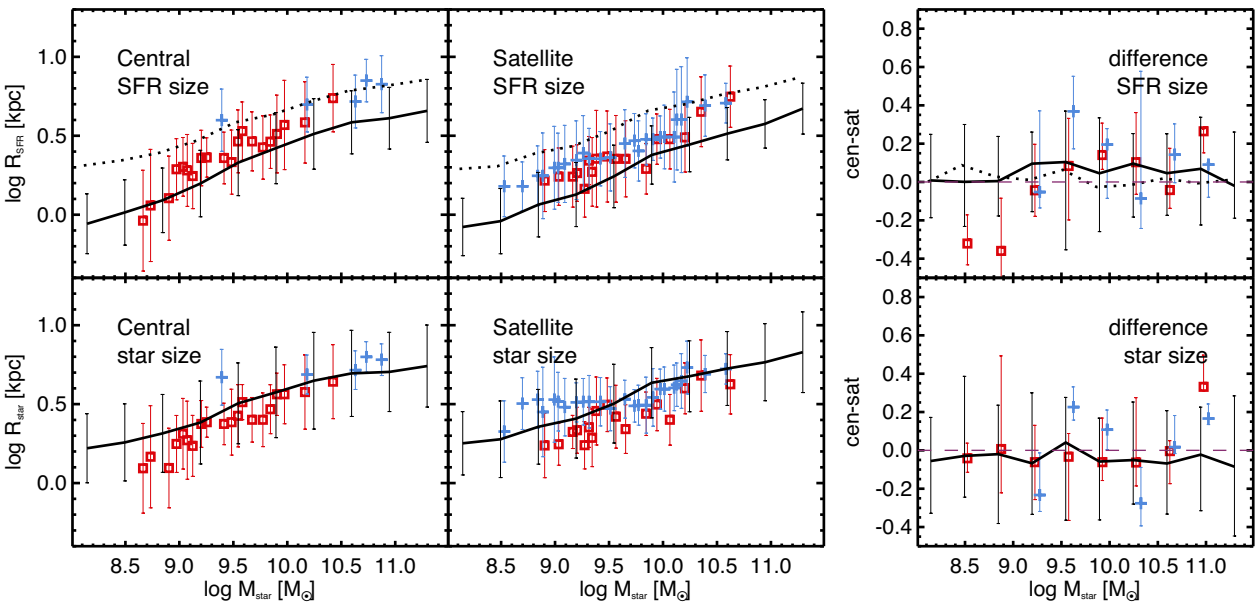

Figure 7. The top and bottom panels show the median size of the star-forming region and of the stellar disc as a function of galaxy stellar mass. Left and middle columns are for centrals and satellites, while the right column shows the difference between centrals and satellites. Symbols and lines have the same meaning as in Fig. 2. The solid and dotted lines in the top panels correspond to the size of the model star-forming region and of the model gaseous disc, respectively.

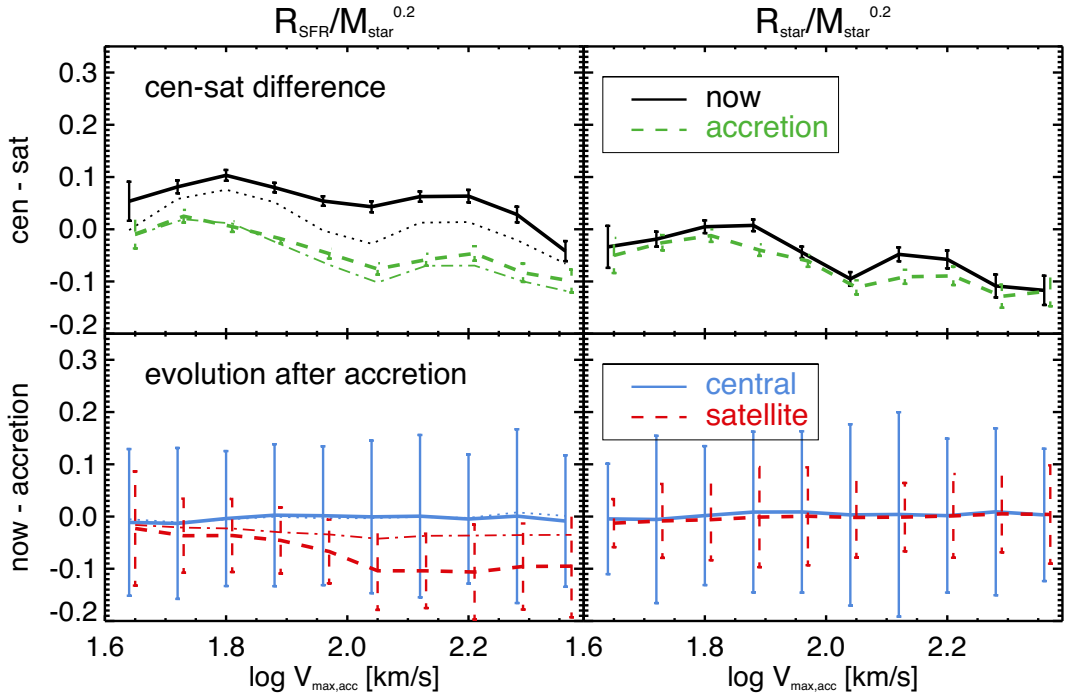

Figure 8. Top panels show the differences between the normalized SF (left) and stellar (right) radii of central and satellite galaxies at present (black solid) and at accretion time (green dashed). In the left panel, black dotted and green dot–dashed lines show the differences for the gaseous disc radii. Bottom panels show the differences between the properties predicted at present and at the time of accretion. Solid blue and dashed red lines correspond to central and satellite galaxies, respectively. Blue dotted and red dot–dashed lines show results for gaseous disc radii of central and satellite galaxies.

of the normalized SF radii and of the gaseous disc radii for central and satellite galaxies. The evolution of the SF radii of central galaxies corresponds to the redshift evolution of the R_{SF}–stellar mass relation predicted by the model. Since accretion, the SF radii and the gaseous disc radii of central galaxies have increased only slightly. For satellite galaxies, the gaseous disc size remains stable, while the SF radii decreases by ∼0.1 dex. As explained above, the evolution of the SF radius follows, in our model, that of the entire gaseous disc. Once a galaxy is accreted, gas cooling (the main driver for the evolution of the gaseous disc, as discussed in Section 4.1) is suppressed so that the gaseous disc size remains stable. The SF radii of satellite galaxies, however, decrease due to star formation that slowly uses up the residual cold gas reservoir. The gas density decreases, leading to a decrease of the H_2-to-HI ratio at all radii, and eventually to a decrease of the star-forming region size.

The right column shows the corresponding results for the stellar radii. The top right panel shows that the difference between stellar radii of central and satellite galaxies are very small. This is due to the fact that (i) the difference at accretion is very small and (ii) the difference barely changes after accretion. As we will discuss in more detail in Section 5.2, point (i) can be explained by the similar assembly history of the host haloes of central and satellite galaxies before accretion. Point (ii) can instead be explained by the lack of significant evolution for the stellar radii of both centrals and satellites after accretion, as shown in the bottom right panel.

Our results show that our model can reproduce the observed SF radii difference between central and satellite galaxies considering only strangulation. The central–satellite difference is partly due to the effect of strangulation on satellite galaxies (i.e. it prevents the gaseous disc size from growing further because cooling is suppressed), and partly a natural consequence of the modelling we have adopted for the partition of cold gas in its atomic and molecular gas components.

5 DISCUSSION

5.1 Model limitations and possible improvements

In Section 3, we have shown that our model satellites deplete their H_2 reservoir more efficiently than their HI content. This results in a too rapid suppression of their star formation activity with respect to expectations based on observational data. We expect that ram-pressure stripping of cold gas, that is not accounted for in our current model version, and a non-instantaneous stripping of the hot gas reservoir, could bring our model predictions into better agreement with data. Below, we elaborate on this in more detail.

In the model, a satellite galaxy suffering strangulation loses gas (via star formation) with no modification of the gaseous disc size. The gas density decreases at all radii, which decreases the molecular fraction. So it is possible to find model satellites with large HI discs but no significant ongoing star formation. Observational data suggest that galaxies residing in denser environments (that can be identified as satellite galaxies) tend to be HI-deficient (Boselli & Gavazzi 2006, and references therein), and are typically more depleted of their HI content than molecular gas (Fumagalli et al. 2009; Boselli et al. 2014b). This is expected because atomic hydrogen is typically more extended than H_2, and should be more easily stripped from galaxies travelling at high speed through the diffuse intra-cluster medium. So the expectation (and this seems supported by data) is that the outer gas disc edge is truncated, while the central regions are unaffected and still characterized by a high

molecular ratio, and therefore active star formation. In our model galaxies, the molecular fraction depends on gas density so that the H I disc is indeed more extended than the molecular disc. By including an explicit treatment for ram-pressure stripping of cold gas, and lowering the efficiency of strangulation, model galaxies should deplete their H I reservoir earlier (and more efficiently) than their molecular gas content. In this scenario satellite galaxies would also have longer quenching time-scales, because star formation can be sustained for longer times by the existing molecular reservoir, and by replenishment with new gas cooling from the hot gas reservoir. We plan to test this scenario in future work.

5.2 Correlation between H I mass and gas size

We find that central galaxies have smaller H I masses and gas radii than their satellite counterparts at accretion time (see Figs 3 and 8). The differences are due mainly to early-accreted galaxies. Our model satellites have been accreted between $0 < z_{\rm acc} < 1$. We find that satellite galaxies that are accreted before $z \sim 0.5$ have larger gas disc radii, and larger H I mass than their central counterparts at the accretion time. The reason is the later formation time of haloes hosting the progenitors of these satellite galaxies with respect to those corresponding to their central counterparts.

Our model predicts a tight correlation between gas disc radii and H I mass for central galaxies, since both properties are related to the assembly history of their host haloes. One quantity that characterizes the halo assembly history is the 'formation time' $f_{\rm halo}$, typically defined as the time when the halo achieves half of its final mass (see detailed discussion in Xie et al. 2015; Zoldan et al. 2018).

The H I mass depends on the halo assembly time, because the H I fraction depends on both the gaseous radius and the total amount of gas available. The latter is tightly correlated to the formation time: galaxies in early-formed haloes tend to have lower gas fraction compared to those in late-formed haloes (see Zoldan et al. 2018 for more detailed discussions). In addition, galaxies in early-formed haloes also have smaller sizes than those in late-formed haloes. In our model, the molecular-to-atomic gas ratio is proportional to the surface gas density:

$$\frac{M_{\rm H2}}{M_{\rm H\,I}} \propto \Sigma_{\rm gas}^{2\alpha} \propto \left(\frac{M_{\rm gas}}{R_{\rm gas}^2}\right)^{2\alpha}$$

with $\alpha = 0.92$ (see Xie et al. 2017). Therefore, galaxies in haloes assembled at early redshifts have higher molecular ratios, and lower H I masses, than those in haloes assembled later.

It is therefore worth noting that our results might depend on the selection. Most of our selected model central/satellite pairs have similar assembly histories. Fig. 9 shows the redshifts corresponding to the halo formation times as a function of halo $V_{\rm max,\,acc}$. We define the $f_{\rm halo}$ as the time when the halo achieves half of its mass at accretion time. The figure shows that the selected centrals and satellites indeed sit in haloes that are formed at comparable times. This leads to comparable SF/stellar radii at accretion time. Therefore the differences of H I mass and sizes between central and satellite galaxies arise after accretion, and can be entirely ascribed to environmental effects.

When using observational data, it is impossible to know if the central and satellite galaxies were in similar environment at earlier epochs so that the biases we have just described might become important.

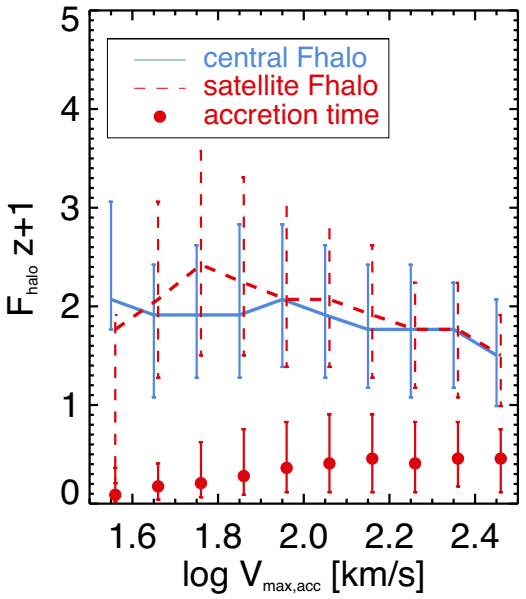

Figure 9. Median formation time of haloes hosting our model galaxies. Blue solid lines and red dashed lines correspond to central and satellite galaxies, respectively. Error bars are the 16, 84 per cent scatters. Red points show the median accretion times for haloes hosting satellite galaxies.

6 CONCLUSIONS

We use the state-of-art semi-analytic model GAEA, together with observational measurements from the HRS, xGASS and HAGGIS surveys to study the gas content and SF/stellar disc sizes of star-forming galaxies (these are selected according to their offset from the model/observed main sequence.). In particular, we focus on the differences between central and satellite galaxies with the aim to determine when and how these differences arise.

The overall distributions of H I and H_2 masses, SFRs, SF and stellar radii of model galaxies agree relatively well with those of observed galaxies. Comparing the median scaling relations of central and satellite star-forming galaxies separately, we find that the different data sets considered are consistent with each other. The model reproduces reasonably well the measured HI mass–stellar mass relation, stellar size–stellar mass relations for both central and satellite galaxies, while predicting a lower normalization for the H_2 mass–stellar mass, SFR–stellar mass, and SF size–stellar mass relations.

For the H I mass, H_2 mas, SFR, and SF radii, the measured differences between central and satellite galaxies are ∼0.2, ∼0.5, ∼0.5, ∼0.1, respectively. No significant difference is measured for the stellar radii. The model agrees well with the observational data for the differences in H I mass, and SF/stellar radii, while significantly overpredicting the differences in H_2 mass and SFR. For our model galaxies, we use the available galaxy merger trees to verify if differences between central and satellite galaxies result from environmental processes or originate before environment starts playing a role. We find that all differences considered can be ascribed to environmental effects, which reduces to stripping of the hot-gas reservoir in our model.

The stellar and gaseous sizes of satellite galaxies in our model are comparable to those of their central counterparts at both accretion time and present time. This is due to the similar assembly history of their host haloes, which is a result of the selection/matching adopted for central–satellite pairs. In our model, the size growth

of star-forming galaxies is dominated by cooling in the case of the gaseous stellar discs, and by subsequent star formation for the stellar discs. Mergers and disc instabilities play a minor role in the size growth of our model galaxies. After accretion (i.e. the time when a central galaxy is accreted on to a larger halo, becoming a satellite galaxy), sizes stop growing because of the suspension of cooling and of the low fraction of stars formed. Meanwhile, central galaxies grow very little at late time.

Including only strangulation, our model reproduces well the median observed H I masses, SF radii, and stellar radii for both central and satellite main sequence (star-forming) galaxies. In contrast, it tends to overpredict the depletion of molecular gas and the related suppression of the star formation activity. We argue that this could be largely resolved with the inclusion of a proper treatment for ram-pressure stripping of the cold gas and for non-instantaneous stripping of hot gas. A treatment of angular momentum balance that accounts for the multi-phase nature of the gaseous disc is also required. We plan to work on these aspects in the future.

ACKNOWLEDGEMENTS

6 ACKNOWLEDGEMENTS

LX and GDL acknowledge financial support from the MERAC foundation. DW and MF acknowledge the support of the Deutsche Forschungsgemeinschaft (DFG) under Project ID 3871/1-1 and ID 3871/1-2. We thank Alessandro Boselli for the help on using the HRS data. We also thank the anonymous referee for comments and suggestions that improved the manuscript significantly.

REFERENCES

Bahé Y. M., McCarthy I. G., 2015, MNRAS, 447, 969
Balogh M. L., Morris S. L., Yee H. K. C., Carlberg R. G., Ellingson E., 1999, ApJ, 527, 54
Bamford S. P. et al., 2009, MNRAS, 393, 1324
Bellhouse C. et al., 2017, APJ, 844, 49
Bennett C. L. et al., 2013, ApJS, 208, 20
Blitz L., Rosolowsky E., 2006, ApJ, 650, 933
Boselli A., Gavazzi G., 2006, PASP, 118, 517
Boselli A., Lequeux J., Gavazzi G., 2002, A&A, 384, 33
Boselli A. et al., 2010, PASP, 122, 261
Boselli A., Cortese L., Boquien M., 2014a, A&A, 564, A65
Boselli A., Cortese L., Boquien M., Boissier S., Catinella B., Gavazzi G., Lagos C., Saintonge A., 2014b, A&A, 564, A67
Boselli A., Fossati M., Gavazzi G., Ciesla L., Buat V., Boissier S., Hughes T. M., 2015, A&A, 579, A102
Bothun G. D., Sullivan W. T., III, 1980, ApJ, 242, 903
Boylan-Kolchin M., Springel V., White S. D. M., Jenkins A., Lemson G., 2009, MNRAS, 398, 1150
Brown T. et al., 2017, MNRAS, 466, 1275
Catinella B. et al., 2013, MNRAS, 436, 34
Catinella B. et al., 2018, MNRAS, 476, 875
Cayatte V., van Gorkom J. H., Balkowski C., Kotanyi C., 1990, AJ, 100, 604
Cayatte V., Kotanyi C., Balkowski C., van Gorkom J. H., 1994, AJ, 107, 1003
Chamaraux P., Balkowski C., Gerard E., 1980, A&A, 83, 38
Chung A., van Gorkom J. H., Kenney J. D. P., Crowl H., Vollmer B., 2009, AJ, 138, 1741
Cora S. A. et al., 2018, MNRAS, 479, 2
Cortese L. et al., 2010, A&A, 518, L49
Cortese L. et al., 2012, A&A, 544, A101
Danovich M., Dekel A., Hahn O., Ceverino D., Primack J., 2015, MNRAS, 449, 2087
De Lucia G., Weinmann S., Poggianti B. M., Aragón-Salamanca A., Zaritsky D., 2012, MNRAS, 423, 1277
De Lucia G., Tornatore L., Frenk C. S., Helmi A., Navarro J. F., White S. D. M., 2014, MNRAS, 445, 970
Dressler A., 1980, ApJ, 236, 351
Emerick A., Mac Low M.-M., Grcevich J., Gatto A., 2016, ApJ, 826, 148
Fabello S., Kauffmann G., Catinella B., Li C., Giovanelli R., Haynes M. P., 2012, MNRAS, 427, 2841
Fossati M. et al., 2013, A&A, 553, A91
Fossati M. et al., 2017, ApJ, 835, 153
Fumagalli M., Krumholz M. R., Prochaska J. X., Gavazzi G., Boselli A., 2009, ApJ, 697, 1811
Gavazzi G., Contursi A., Carrasco L., Boselli A., Kennicutt R., Scodeggio M., Jaffe W., 1995, A&A, 304, 325
Gavazzi G., Boselli A., Scodeggio M., Pierini D., Belsole E., 1999, MNRAS, 304, 595
Giovanelli R., Haynes M. P., 1985, ApJ, 292, 404
Giovanelli R. et al., 2005, AJ, 130, 2598
Gómez P. L. et al., 2003, ApJ, 584, 210
Gunn J. E., Gott J. R., III, 1972, ApJ, 176, 1
Guo Q. et al., 2011, MNRAS, 413, 101
Guo Q., White S., Angulo R. E., Henriques B., Lemson G., Boylan-Kolchin M., Thomas P., Short C., 2013, MNRAS, 428, 1351
Haynes M. P. et al., 2011, AJ, 142, 170
Hirschmann M., De Lucia G., Wilman D., Weinmann S., Iovino A., Cucciati O., Zibetti S., Villalobos Á., 2014, MNRAS, 444, 2938
Hirschmann M., De Lucia G., Fontanot F., 2016, MNRAS, 461, 1760
Jáchym P. et al., 2017, ApJ, 839, 114
Jaffe W., 1983, MNRAS, 202, 995
Jaffé Y. L. et al., 2016, MNRAS, 461, 1202
Kauffmann G., White S. D. M., Heckman T. M., Ménard B., Brinchmann J., Charlot S., Tremonti C., Brinkmann J., 2004, MNRAS, 353, 713
Kenney J. D. P., van Gorkom J. H., Vollmer B., 2004, AJ, 127, 3361
Koopmann R. A., Kenney J. D. P., 2004, ApJ, 613, 866
Koopmann R. A., Haynes M. P., Catinella B., 2006, AJ, 131, 716
Kuchner U., Ziegler B., Verdugo M., Bamford S., Häußler B., 2017, A&A, 604, A54
Kulkarni S., Wilman D., Erwin P., Koppenhöfer J., Gutierrez L., Beckman J., Saglia R., Bender R., 2014, in Seigar M. S., Treuthardt P., eds, ASP Conf. Ser. Vol. 480, Structure and Dynamics of Disk Galaxies. Astron. Soc. Pac., San Francisco, p. 255
Larson R. B., Tinsley B. M., Caldwell C. N., 1980, ApJ, 237, 692
Lewis I. et al., 2002, MNRAS, 334, 673
Luo Y., Kang X., Kauffmann G., Fu J., 2016, MNRAS, 458, 366
Martin D. C. et al., 2005, ApJ, 619, L1
Merritt D., 1983, ApJ, 264, 24
Mo H. J., Mao S., White S. D. M., 1998, MNRAS, 295, 319
Moore B., Katz N., Lake G., Dressler A., Oemler A., 1996, Nature, 379, 613
Morrissey P. et al., 2007, ApJS, 173, 682
Odekon M. C. et al., 2016, ApJ, 824, 110
Peng Y.-j., Lilly S. J., Renzini A., Carollo M., 2012, ApJ, 757, 4
Planck Collaboration et al., 2015, A&A, 594, A13
Poggianti B. M., Smail I., Dressler A., Couch W. J., Barger A. J., Butcher H., Ellis R. S., Oemler A., Jr., 1999, ApJ, 518, 576
Saintonge A. et al., 2017, ApJS, 233, 22
Schaefer A. L. et al., 2017, MNRAS, 464, 121
Solanes J. M., Manrique A., García-Gómez C., González-Casado G., Giovanelli R., Haynes M. P., 2001, ApJ, 548, 97
Speagle J. S., Steinhardt C. L., Capak P. L., Silverman J. D., 2014, ApJS, 214, 15
Spindler A., Wake D., 2017, MNRAS, 468, 333
Springob C. M., Haynes M. P., Giovanelli R., Kent B. R., 2005, ApJS, 160, 149
Steinhauser D., Schindler S., Springel V., 2016, A&A, 591, A51
Stevens A. R. H., Lagos C. d. P., Contreras S., Croton D. J., Padilla N. D., Schaller M., Schaye J., Theuns T., 2017, MNRAS, 467, 2066
Tecce T. E., Cora S. A., Tissera P. B., Abadi M. G., Lagos C. D. P., 2010, MNRAS, 408, 2008

Tonnesen S., Bryan G. L., 2009, ApJ, 694, 789
Tonnesen S., Bryan G. L., 2010, ApJ, 709, 1203
Wang J., De Lucia G., Kitzbichler M. G., White S. D. M., 2008, MNRAS, 384, 1301
Wang J. et al., 2011, MNRAS, 412, 1081
Weinmann S. M., Kauffmann G., van den Bosch F. C., Pasquali A., McIntosh D. H., Mo H., Yang X., Guo Y., 2009, MNRAS, 394, 1213
Wetzel A. R., Tinker J. L., Conroy C., van den Bosch F. C., 2013, MNRAS, 432, 336
Wright E. L. et al., 2010, AJ, 140, 1868
Xie L., Guo Q., Cooper A. P., Frenk C. S., Li R., Gao L., 2015, MNRAS, 447, 636
Xie L., De Lucia G., Hirschmann M., Fontanot F., Zoldan A., 2017, MNRAS, 469, 968
Yang X., Mo H. J., van den Bosch F. C., Pasquali A., Li C., Barden M., 2007, ApJ, 671, 153
Zibetti S., Charlot S., Rix H.-W., 2009, MNRAS, 400, 1181
Zoldan A., De Lucia G., Xie L., Fontanot F., Hirschmann M., 2018, preprint (arXiv:1803.08056)

This paper has been typeset from a TEX/LATEX file prepared by the author.